IEEE INSTRUMENTATION & MEASUREMENT SOCIETY

Received 6 July 2022; accepted 2 August 2022. Date of publication 15 August 2022; date of current version 7 September 2022.
The review of this article was arranged by Associate Editor Samir Trabelsi.

Digital Object Identifier 10.1109/OJIM.2022.3198483

Crack Detection and Corrosion Mapping Using Loaded-Aperture Microwave Probe

MOHAMMED SAIF UR RAHMAN, OMAR S. HASSAN, AND MOHAMED A. ABOU-KHOUSA (Senior Member, IEEE)

Electrical Engineering and Computer Science Department, Khalifa University of Science and Technology, Abu Dhabi, UAE

CORRESPONDING AUTHOR: M. S. U. RAHMAN (e-mail: mohammed.urrahman@ku.ac.ae)

This work was supported by the Khalifa University of Science and Technology, Abu Dhabi, UAE, under Award CIRA-2020-037.

ABSTRACT Employing circular aperture probes for microwave imaging in the near-field has been proven to render high resolution images of a variety of samples under test (SUT) when compared to the conventionally utilized rectangular aperture probes. In this paper, it is proposed to further enhance the near-field imaging resolution and sensitivity by loading the circular aperture (operating in the K-band frequency range) with a resonant iris. It is shown that the probe exhibits a confined and localized near-field distribution close to the iris opening, thereby improving its resolution and sensitivity. The design and analysis of the probe presented herein are aided by 3D electromagnetic simulations and validated experimentally. The spatial resolution of the probe is established through line scans of the probe over a pair of targets interspaced at known distances. To further demonstrate the utility of the probe in critical non-destructive testing (NDT) applications, a manufactured prototype is devised to detect cracks on metal structures and map corrosion areas hidden under paint layers. It is shown here that the proposed probe provides significant resolution and sensitivity improvement over the un-loaded circular aperture probe. Specifically, for crack detection, the proposed probe provides two-fold and more than three-fold improvement in the resolution and sensitivity, respectively. For corrosion mapping, the proposed probe yields 2 to 5 times higher image signal-to-noise ratio compared to the unloaded aperture probe.

INDEX TERMS Circular probe, cracks, corrosion, iris structure, microwave imaging, non-destructive testing, resonant sensor.

I. INTRODUCTION

HIGH-RESOLUTION near-field microwave imaging methods are emerging as powerful inspection tools for diverse industrial applications. These methods have been successfully applied for non-destructive testing (NDT) of metal structures to detect surface defects such as cracks [1], [2], [3], [4], [5], [6], [7], [8], [9] and precursor pits [10], [11], map corrosion and rust under paint [12], [13], and inspect composite materials for subsurface defects [14], [15], [16], [17], among others. For these applications, the practical utility of near-field microwave imaging as an inspection modality and its merits compared to other well-known NDT modalities such as phased array ultrasonic testing have been demonstrated recently [14], [16].

Microwave imaging probes operating in the near-field, reported in the past include coaxial probes [18], [19], [20], printed planar imaging probes [17], [21], [22], [23], [24], [25], bulk periodic left-handed metamaterial (LHM) super lens [26], [27], non-periodic near-field plates [28], [29], waveguide-fed aperture probes [10], [11], [12], [13], [14], [15], [16], [30], [31], [32] and aperture probes loaded with resonant structures [2], [7], [33], [34], [35], [36]. The main design objectives of probes operating in the near-field are to enhance the lateral resolution and sensitivity. This is accomplished generally by confining the electromagnetic (EM) fields in the probe's near-field region [26].

Rectangular and circular apertures fed by waveguides have been utilized thoroughly as near-field imaging probes for numerous industrial applications [6], [14], [30], [37]. These

probes are typically devised for imaging as they are relatively inexpensive and easy to fabricate. Unlike most of other near-field probes, these apertures emit near fields that are limited to a tiny footprint in the near-field area and maintained for greater imaging distances. In essence, the resolution capability of the probe is determined by the lateral size of its footprint in the near-field. It is well-established that the attainable lateral resolution from aperture near-field probes is around half the largest dimension of the aperture [38], [39]. The resolution of aperture probes can be further enhanced by loading the feeding waveguide with low-loss dielectric materials [7], [10], [40], [41] and tapering the feeding waveguide to yield a smaller aperture [10], [38], [42].

Recently, loading waveguide-fed rectangular apertures with resonant structures have been shown to significantly enhance resolution of the probe (in the near-field) [2], [7], [33], [34], [35], [36], [43]. Electrically-small split-ring resonators were employed in [2] and [36] to load rectangular apertures. However, the capability of the previously developed probes were either not demonstrated for corrosion under paint mapping and/or thin crack detection.

In this paper, a waveguide-fed circular aperture probe operating at 26 GHz is introduced for crack detection and corrosion mapping. A resonant iris structure is attached to the aperture of the probe proposed herein. Owing to the confined footprint of the probe in the near-field region, the spatial resolution and detection sensitivity are enhanced. The design of the proposed probe is relatively simple and practically feasible. Although the used iris structure has been known since long time ago [44], it was only recently devised to load a circular aperture and demonstrated for imaging of composite structures in the X-band frequency range [45]. On the other hand, experimental investigations revealed the inadequacy of the aforementioned probe in detection of practical corrosion under paint samples and limited resolution for cracks with narrow spacing between them. The efficacy of such an iris loaded probe operating at a higher frequency band for crack and corrosion under paint detection is yet to be demonstrated In this work, the iris loaded circular aperture probe that operates at a relatively higher frequency (K-band) is introduced and its effectiveness towards detection of cracks and corrosion under paint is presented. The analysis and evaluation of the designed probe is supported by extensive electromagnetic simulations and experimental investigations.

The remainder of the paper is organized as follows. Section II describes the design of the proposed probe along with a comprehensive characterization of its performance through electromagnetic simulations. Experimental results demonstrating the resolution and sensitivity of the probe, along with the acquired images of corrosion under paint samples are included in Section III. Conclusions and remarks of the overall work is summed up in Section IV.

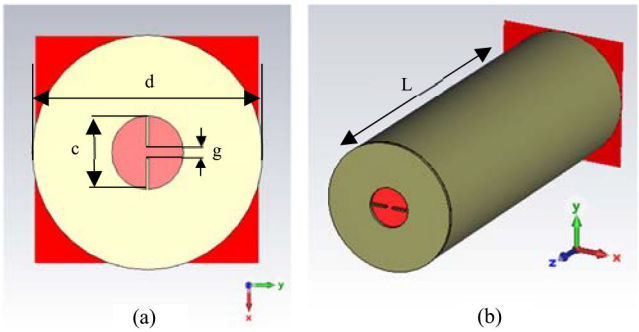

FIGURE 1. 3D model of the simulated probe showing (a) the iris in front and (b) the probe in perspective view.

TABLE 1. Iris probe simulation parameters and description.

Parameter	Value	Description
d	10.8 mm	Outer diameter of iris cap
L	30.00 mm	Circular probe length
g	0.545 mm	Strip gap
c	3.38 mm	Iris slot diameter
w	0.29 mm	Iris strip width
t	0.32 mm	Iris wall thickness

II. PROBE DESIGN AND SIMULATIONS

The K-band probe introduced in this paper is a resonant iris loaded circular aperture fed with a waveguide, as shown in Fig. 1. A zoomed in picture of the resonant iris structure and a perspective view of the probe modeled in CST (Computer Simulation Technology) Studio Suite [46] are illustrated in Fig. 1(a) and (b) respectively.

The resonant iris structure is built out of aluminum. It has sub-resonant circular slot of diameter of 3.38 mm and a pair of 0.29 mm wide strips extending from the edge of the slot to the center. A gap of 0.545 mm is maintained between the strips, which adds the capacitance required to create resonance by the iris structure. The thickness of the iris wall is 0.32 mm. The iris structure is attached to the aperture of a 30 mm long circular waveguide probe (made of aluminum as well) with internal diameter of 6.25 mm. The circular probe is loaded with Teflon to reduce the cut-off frequency in the circular waveguide.

The geometrical parameters of the iris structure and the circular probe considered for simulation are tabulated in Table 1. In simulation, a waveguide port was used to feed the probe such that the electric field is along the strips of the iris. The model was simulated under free-space conditions using the FD (frequency domain) solver to acquire its response which is shown in Fig. 2. The figure depicts the magnitude of the reflection coefficient (S_{11}) as a function of frequency. It can be observed that the probe resonates close to 26 GHz and has magnitude of -17.2 dB. The dip observed around 24 GHz is possibly due to a higher order mode of the probe. The response of a circular aperture probe without the iris structure is also depicted in the figure to show the effect of the resonant iris on the aperture reflection. It is evident that the magnitude of reflection coefficient of the

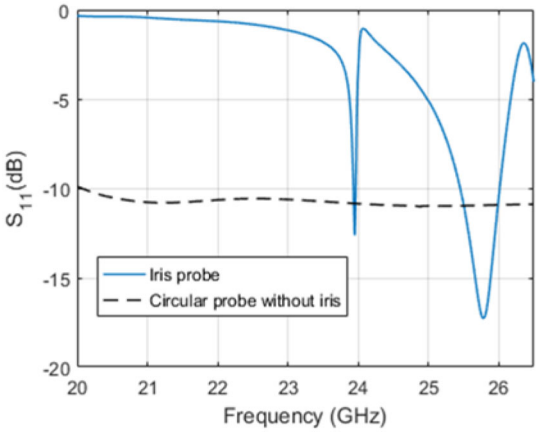

FIGURE 2. Simulated reflection coefficients of circular probe with and without the iris structure radiating into free-space.

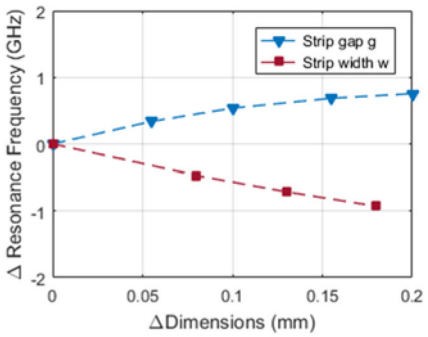

FIGURE 3. Shift in resonance frequency as a function of iris parameter dimensions.

circular probe without the iris is relatively flat throughout the frequency range, while the iris loaded probe resonates sharply at the resonance frequency with better matching. It is further remarked that the reflection coefficient and resonance frequency of the iris probe is affected by changes in the probe design parameters, such as the strip width, the strip gap length, and the slot radius. However, the factor affecting the resonance most was found to be the strip gap between the metal strips of the iris. Several trials involving parametric sweeps of the strip gap and strip width were performed to optimize the iris parameters. Sensitivity analysis for iris parameter dimensions was performed in simulation and is depicted in Fig. 3. The figure presents the shift in resonance frequency as a function of change in nominal values of iris strip gap and strip width. It is evident that increasing the strip gap resulted in a positive change in resonance frequency, while the resonance frequency decreased with any increments in strip width. The final design parameters were therefore fixed based on the best matching obtained for the reflection coefficient of the probe.

A. NEAR-FIELD DISTRIBUTION

As mentioned earlier, the circular probe when loaded with the iris structure causes the near-field distribution to be confined locally near the opening of the iris. To demonstrate

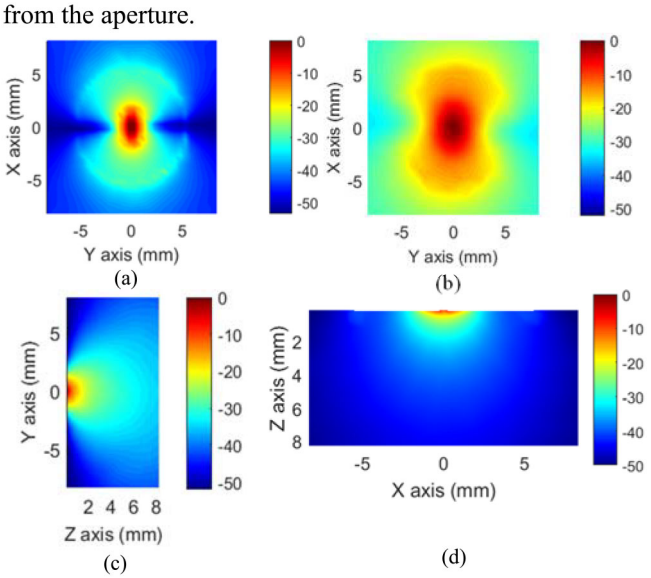

FIGURE 4. Simulated electric field distribution (magnitude) in (a) $x-y$ plane at $z=0$, (b) $x-y$ plane $z=1$, (c) $y-z$ plane at $z=0$, and (d) $x-z$ plane at $z=0$.

this, the electric field distribution (magnitude) of the probe in $x-y$ plane at the aperture of the iris is shown in Fig. 4(a). It is evident from the figure that the electric field intensity is concentrated at the center, which is at the gap between the strips. However, the field intensity attenuates gradually and symmetrically along opposite directions. The magnitude of electric field intensity plot along the $x-y$ plane at a distance of 1 mm from the aperture of the probe is shown in Fig. 4(b). It can be seen that the electric field is relatively less concentrated at the center of the iris when compared to the response at the aperture. This is expected for near-field probes, as the electric field spreads rapidly as a function of standoff distance (SOD) from the aperture. Additionally, the electric field distributions along $y-z$ and $x-z$ planes are also presented in Fig. 4(c) and (d). In the $y-z$ plane, the electric field intensity remains within 25 dB of the maximum at the aperture up to a distance of 2 mm and then gradually attenuates while moving away from the aperture. Moreover, the $x-z$ plane figure shows that the field is concentrated around the iris slot and fades at a distance greater than 2 mm from the aperture.

B. RESOLUTION

To assess the spatial resolution of the probe, a printed circuit board (PCB) sample was modeled in CST. The 1.6 mm thick substrate made of FR-4 was built and a conductive layer was placed on top of the substrate. Thin strips of the conductive layer were removed to emulate narrow cracks on the surface of a conductor as presented in Fig. 5(a). Three pairs of cracks of constant width (0.25 mm) but varying interspacing between each pair were created. The separation among the cracks in the first pair is 1mm (starting from left), while the interspacing among cracks in the next two pairs is 2mm and 3mm respectively. A line scan was performed along the

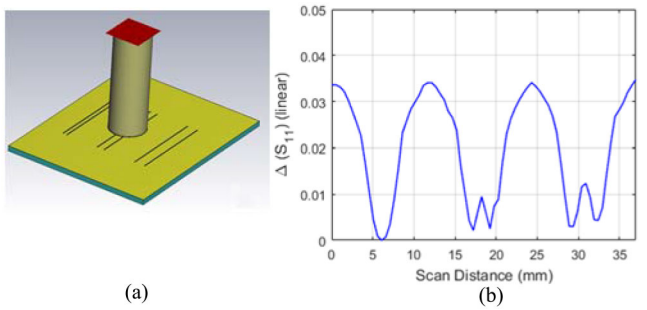

FIGURE 5. (a) Picture of the PCB crack sample developed in CST, and (b) change in magnitude of reflection coefficient (linear) for a line scan over the same sample.

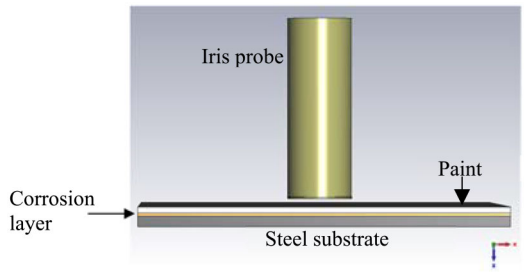

FIGURE 6. Simulation model showing the corrosion layer on steel substrate concealed under paint.

3 pair of cracks having varying interspacing between them (1-3mm), at a standoff distance of 1mm and a step size of 0.5mm. The relative change in magnitude (linear) obtained subsequent to the line scan is shown in Fig. 5(b). It can be observed that the probe produced clear and distinguishable peaks for the 2mm and 3mm spaced cracks, while rendered a single indication for the 1mm spaced pair of cracks. The resolution of the probe, therefore is established at 2 mm from the figure.

C. SENSITIVITY

To assess the performance of the iris probe for detecting corrosion layers under paint, a steel sample with uniform layer of corrosion concealed under paint was created in CST, as presented in Fig. 6. The steel substrate measures 100 by 60 mm and has thickness of 1.7 mm. Initially, only a 1 mm thick layer of paint was applied on the steel substrate. The response of the iris probe and a circular aperture probe without iris was simulated for a frequency range of 20-26.5 GHz at a standoff distance of 1 mm from the painted steel sample. Subsequently, a corrosion layer was introduced beneath the paint layer to mimic a scenario where corrosion forms under paint. The thickness of the corrosion layer was varied between 0.05 mm to 0.2 mm and the response of both probes (with and without iris) was recorded at a given standoff distance (1mm) and over a frequency range of 20-26.5 GHz. The dielectric constants of paint and corrosion layer considered for this simulation are 5.346 – j0.21 and 5.5 – j0.55, respectively [8], [47].

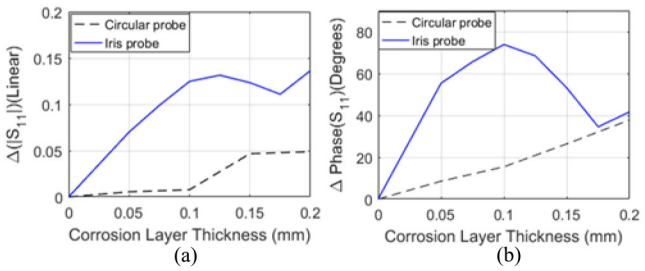

FIGURE 7. Relative change in (a) magnitude and (b) phase from no-corrosion to increasing thickness of corrosion layer produced by the iris probe and circular probe (without iris).

TABLE 2. Change in magnitude and phase for increasing corrosion thickness.

	Iris probe		Circular probe	
Corrosion layer thickness (mm)	ΔMag.	ΔPhase	ΔMag.	ΔPhase
0.025	0.03	27	0.003	4.8
0.05	0.07	55.3	0.005	8.5
0.075	0.1	65.6	0.007	12.2
0.1	0.125	73.8	0.008	15.4
0.125	0.13	68.4	0.03	21.6
0.15	0.12	53.1	0.046	26.4
0.175	0.11	34.5	0.048	32.3
0.2	0.14	41.6	0.05	37.8

The change in the magnitude and phase of the reflection coefficient relative to the no-corrosion case as function of the corrosion layer thickness as obtained from both probes is presented in Fig. 7(a) and (b) (plotted at 25.6 GHz). The corresponding numerical data is represented in Table 2. Referring to the table, the change in magnitude rendered by the circular aperture probe for a corresponding 0.025 mm increase in thickness of corrosion layer (from no-corrosion case) is 0.003, while the iris probe produced a change of 0.03, which is ten times higher. It is remarked that such minute changes (<0.02) are close to the uncertainty of the network analyzer which is employed to carry out measurements. While both probes depicted considerable change in phase for a 0.025 mm increase in corrosion thickness layer, the iris probe showed more than five times higher sensitivity when compared to the circular probe. From the table, it is also evident that the iris probe produced maximum change (in magnitude) for the 0.2 mm thick corrosion layer, which is still almost three times higher than the circular aperture probe. In comparison to the circular probe, for the 0.1 mm thickness layer of corrosion, the iris probe demonstrated more than 15 times higher sensitivity in magnitude and around five times better phase response. However, for the subsequent increase in corrosion layer thickness, the change in phase and magnitude rendered by the iris probe either dipped or remained nearly constant. On the other hand, the circular probe produced roughly six times higher magnitude change for the 0.15 mm thickness layer of corrosion and was constant thereafter. The phase change depicted by the circular probe linearly increased by approximately 1.5 times with the corrosion layer thickness. Nevertheless, the change in magnitude recorded from the iris probe is still more than

FIGURE 8. (a) Photograph of the manufactured probe, and (b) a zoomed in illustration of the iris structure (all dimensions in mm).

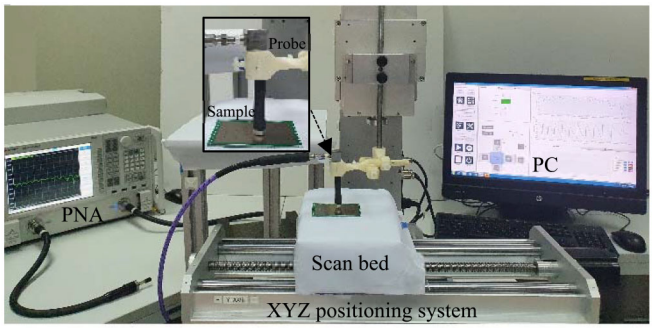

FIGURE 9. Photograph of the imaging setup.

2.5 times higher than the circular probe (for 0.15 mm and 0.2 mm corrosion layer thickness). Moreover, the calculated change in phase from the iris probe is double than the circular probe for 0.15 mm thickness of corrosion and is comparatively higher for the thickest layer considered herein. The iris probe clearly demonstrated higher sensitivity than the circular probe for corrosion under paint, and in particular for thin layers, which is of practical interest in the industry.

III. MEASUREMENT RESULTS

The manufactured prototype of the probe used for measurements in this work is shown in Fig. 8(a), and an enlarged photograph of the resonant iris structure is illustrated in Fig. 8(b).

The dimensions of the as-built iris structure are annotated in the figure. The manufactured iris slot dimeter measures 3.4 mm and width of the metal strips is 0.29 mm, while the strip gap is 0.58 mm, slightly higher than the value considered in simulation. This is attributed to tolerances in manufacturing and material. The iris structure was attached to the circular aperture probe via conductive epoxy. The probe has an external diameter of 10.8 mm.

The overall imaging setup utilized in this work is shown in Fig. 9 with a zoomed in illustration of the probe fixed to the positioning system in the inset. A Network Analyzer (NA) was used to measure the complex reflection coefficient at the feed location of the probe (i.e., at the SMA port). For all the measurements performed herein using the iris probe, the RF input power was -15 dB, and the intermediate frequency bandwidth (IFBW) was set at 10 KHz. It is remarked that although such an IFBW is not very suitable

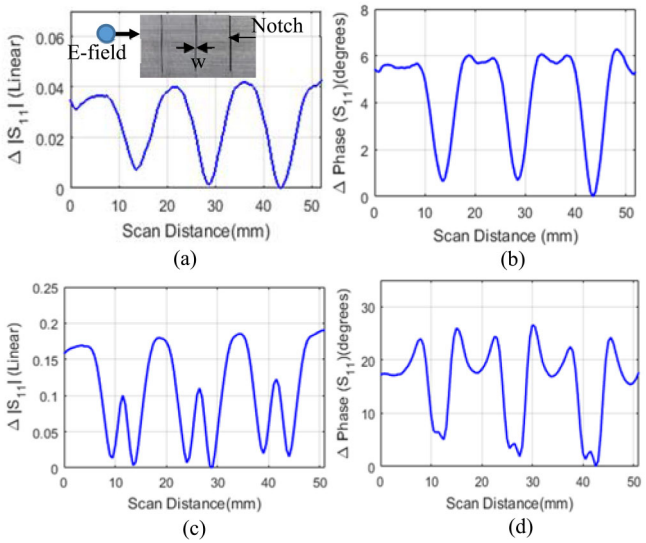

FIGURE 10. Relative change in magnitude and phase produced by (a, b) circular probe with photo of metallic notch sample in the inset and (c, d) iris probe.

for accurate measurements of resonant structures, there is always a hard compromise between speed of operation and RF accuracy/resolution. A frequency range of 20-26.5 GHz was swept over 201 points. An automated scanning table was employed to move the sample in predetermined step sizes and a PC was used to control the table and to plot the scanned data. It is remarked that the XYZ positioning stage used herein addresses a wide range of scanning distances, in contrast with nanoscale set-ups that work on micron scale and requires complicated distance control. The manufactured probe was used for crack detection and mapping of corrosion under paint as presented in the following subsections.

A. CRACK DETECTION

To demonstrate the response of the probe for narrow notches in metals, a sample shown in the inset of Fig. 10(a) was prepared and scanned by the probe. To simulate cracks for the investigation, narrow notches were machined through a 9.5 mm thick aluminum block using the process used in [3]. The notches have equal lengths of 30 mm and width (w) ranges from 0.25 mm to 0.75 mm (left to right), increasing in steps of 0.25 mm. The interspacing between each notch is 15 mm.

Line scans were performed along the notches using the iris probe and a circular aperture probe introduced in [30], [48]. The distance between probes and the sample was fixed at 1 mm (standoff distance). For all scans, a frequency range of 20-26.5 GHz was swept for 201 points along a scan distance of 52 mm. An automated scanning table was employed to move the sample with precise step sizes of 0.5 mm along the scan direction. Both probes were positioned such that the electric field orientation is orthogonal to the notch width.

The change in magnitude and phase (relative to the response without notch) as obtained using the circular probe were used to produce the line scans shown in Fig. 10(a)

and (b), respectively. Distinct indications were produced for each notch in the sample. The relative changes in magnitude and phase are shown to be proportional to increase in notch width. The change in magnitude for the 0.25 mm wide notch is around 0.03 (linear) and the corresponding phase change is roughly 5.3 degrees. The maximum change in magnitude for the widest notch is 0.043, and the phase changes by 6.3 degrees, increasing only slightly from the change observed for the 0.5 mm notch (0.04 in magnitude and 5.6 degrees in phase).

The results from the line scan of the metallic notch sample generated by the proposed iris probe are shown in Fig. 10(c) and (d). Strong indications were produced for each notch. While the change in magnitude (linear) measured around 0.17, a phase change of almost 20.5 degrees was observed for a notch width of 0.25 mm. For the widest notch (0.75 mm), the iris probe produced a change of 0.18 in the magnitude and an approximate 24.3 degree change in phase. Similar to the circular probe response, the difference in the magnitude and phase change for the 0.5 mm and 0.75 mm wide notch is minimal. In contrast to the circular aperture probe, the iris probe rendered roughly 6 times more change in magnitude for the narrowest notch (0.25 mm) and the relative change in phase was almost four times. For the widest notch, the change in magnitude and phase is close to four times that of the circular probe response, thereby highlighting the higher sensitivity of the iris probe.

It is observed that the iris probe yields double indications for each notch, which are manifested in the magnitude response. These are attributed the null in the electric field at the center of the iris structure while radiating over the notch on the metal surface. To confirm this, the electric field distributions of the probe when radiating over a metal block with and without notch are presented. A metal sample with a narrow notch of width 0.25 mm (resembling the sample in Fig. 10(a)) was created in CST simulation environment. The normalized electric field distribution (magnitude) along the metal strips of the iris when radiating over the notch is shown in Fig. 11(a). It is apparent from the figure that electric field null exists at the center of the iris structure (opening gap of the strips), which explains the double indications rendered by the probe in Fig. 10(c). The field seems to be more confined while the probe is radiating over the notch and it is relatively more dispersed when there is no notch as evident in Fig. 11(b). It is further remarked that, double indications in the probe response are in fact advantageous and have been reported to increase the probability of detection [11].

To assess the spatial resolution of the probe, a crack sample was prepared on a PCB substrate as shown in Fig. 12(a). The sample is a manufactured prototype of the model demonstrated in the simulation (c.f. Fig. 5(a)). The PCB is made out of FR-4 material with thickness of 1.6 mm. Cracks of equal length of 25 mm were etched on the copper layer. In line with the simulation model, three pairs of cracks with different interspacing between them were created. The

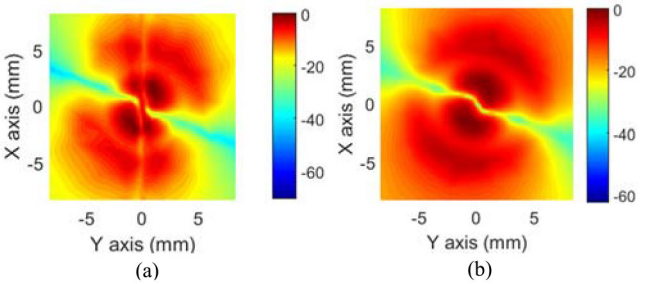

FIGURE 11. Simulated electric field distribution (magnitude) of the probe in $x - y$ plane at a standoff distance of 1mm from the (a) notch on metal surface and (b) without notch.

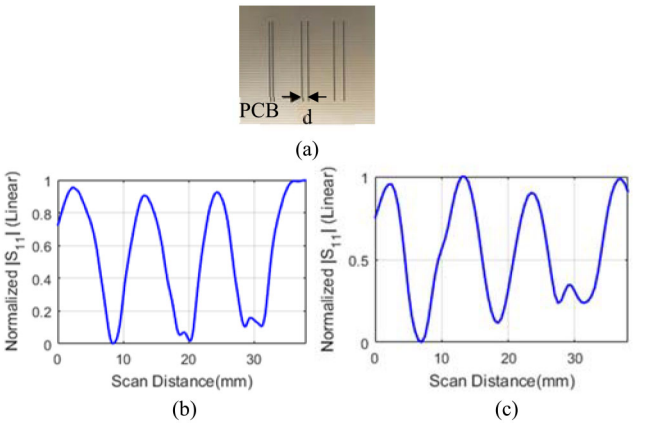

FIGURE 12. (a) Picture of the PCB sample, and normalized magnitude line scans (linear) rendered by the (b) iris probe and the (c) X-band probe proposed in [45].

interspacing distance (d) between cracks in each pair is 1mm, 2mm, and 3mm, as annotated in the figure.

The iris probe and the X-band probe proposed in [45] were utilized to conduct line scans over the pair of cracks such that the electric field was orthogonal to the crack width. The standoff distance from the aperture of the probes and the sample was fixed at 1 mm and the step size with which the sample moved beneath the probes was 0.5 mm. The normalized magnitude response of the iris probe and the probe introduced in [45] is shown in Fig. 12(b) and (c) respectively. It is perceivable that the proposed probe rendered two clear distinct peaks for the 2 mm spaced cracks. This is in line with the simulated line scan result of the probe over a similar PCB crack sample modeled in CST (c.f. Fig. 5(b)). It is therefore established both in simulation and measurement that the spatial resolution of the probe is 2 mm. This is a twofold improvement over the unloaded aperture probe which rendered 4 mm resolution [30]. However, the probe introduced in [45] failed to resolve the 2mm spaced cracks and only rendered clear distinction for the 3mm spaced cracks.

To demonstrate the capability of the proposed probe towards narrow crack detection, two samples were prepared. The first sample is a PCB substrate, similar to the one shown in Fig. 12(a). Slits of same length, but varying width were etched on the copper layer as shown in Fig. 13(a). The

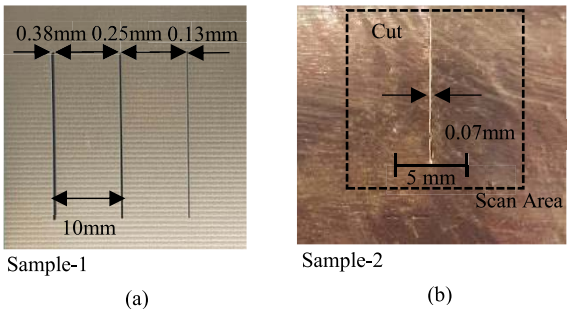

FIGURE 13. Photograph of (a) PCB sample with varying slit width (sample-1) and (b) zoomed 0.07 mm wide cut on a copper tape sheet (sample-2).

smallest slit width on this sample measures 0.13 mm. The second sample was prepared using a sheet of copper tape of nominal thickness 0.08 mm. A very fine cut of width 0.07mm was made on the surface of the sheet via a thin knife, as depicted in a zoomed in photograph of the sample presented in Fig. 13(b).

Both samples were imaged using the proposed iris probe using the imaging setup shown in Fig. 9. The probe was fixed at a standoff distance of 1 mm from the sample surface and moved along the scan area with step size of 0.5 mm along each axis. Normalized magnitude and phase images of the first sample rendered by the probe are shown in Fig. 14(a) and (b) respectively. The images were plotted at 26.2 GHz. As evident, all three slits were produced by the probe and notably the narrowest slit of the sample measuring only 0.13 mm. While the slits are visible in both magnitude and phase images, the magnitude image presents the slits with clear distinction from the background.

The normalized magnitude and phase image of the second sample is depicted in Fig. 14(c) and (d) respectively. The rendition of the fine cut of width 0.07 mm was clearly portrayed in the image. Similar to the previous sample, the magnitude image offers a better contrast to the background when compared to the phase image. The length of the cut is also faithfully reproduced in the images, with clear demarcation of the extremities.

To benchmark the crack detection capability of the probe against previously published work, the minimum crack width detected using the proposed probe is compared to other works in Table 3. It is to be noted that the minimum crack width detected in this work (0.07 mm) is lesser than most works reported earlier. From the table, it can be seen that only in [36], a lesser width than the one presented herein was detected. However, it is also remarked that the standoff distance between the probe and the sample was almost half when compared to this work. In fact, none of the papers in Table 3 demonstrated crack detection at such SOD (1 mm). Apart from this, there are papers in which cracks with lesser width were detected. However, either the imaging was performed at a very high frequency [55] or different approaches like the higher order mode (HOM)/contact methods were adopted [56].

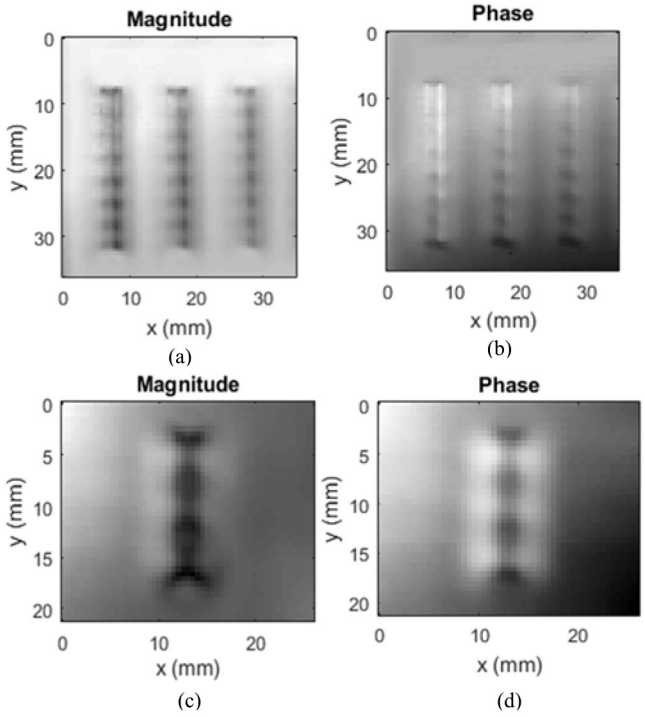

FIGURE 14. Normalized magnitude and phase images of (a,b) sample-1 and (c,d) sample-2.

TABLE 3. Example crack width detection in some of the previous works.

Ref.	Probe Type	Freq. (GHz)	Notch Width (mm)	SOD (mm)
[4]	Complementary split-ring resonator(CSRR)	5	0.1	0*
[49]	Microstrip line resonator and dual-behavior resonator (DBR) band-pass filter probe	13	0.2	0.05
[36]	Rectangular Waveguide loaded with Linear Array of Circular SRRs	16.65	0.0254#	0.6
[50]	Open-ended coaxial line sensor	14-18	0.26	0*
[51]	Open-ended Rectangular Waveguide	9.4	3.2	0.3
[52]	Open-ended Rectangular Waveguide	8.2-12.4, 18-40	0.5	0*
[53]	Array waveguide probe	12.5, 24	0.25	0.5
[54]	Substrate integrated waveguide (SIW) cavity and a complementary split ring resonator(CSRR)	5	1	0.1
This work	Circular aperture probe loaded with resonant iris	26	0.07	1

*in contact, #spliced metal boards
Note: Multiple other works have detected much tighter cracks using near-field techniques.

B. CORROSION MAPPING

To demonstrate the sensitivity of the probe in corrosion mapping application, two samples were considered. The photos shown in Fig. 15 show the samples with 1 mm thick paint layer applied over them and with scan area highlighted.

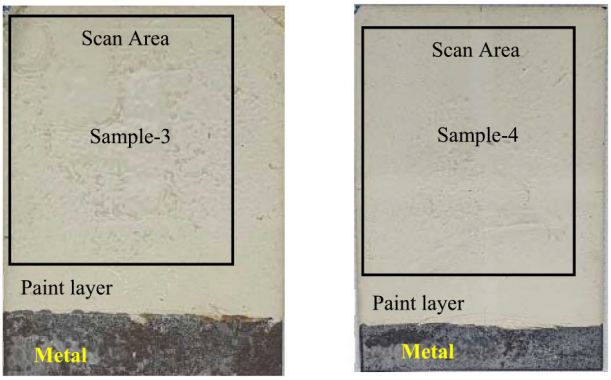

FIGURE 15. Photos of the corrosion samples covered under paint.

The first sample in this sub-section (Sample-3) has a number "4" engraved in the metal. It was left to corrode naturally, and then, it was painted. The second sample (Sample-4) had a localized corrosion layer under the paint [16].

A scan was performed over the samples using the iris probe and the circular aperture probe at a standoff distance and step size of 1mm. The normalized magnitude and phase images of sample-3 obtained using both probes are depicted in Fig. 16. The engraved number "4" is clearly visible in all the images with clear distinction from the background. However, in the images acquired using the circular probe, the engraved impression is not as sharp as indicated by the iris probe image. This is attributed to high resolution and sensitivity of the iris probe, which is noticeable in the images.

To compare the performance of the probes in quantitative terms, the signal-to-noise ratio (SNR) value of the images produced by both probes was calculated using the approach reported in [14] and is presented in Table 3. For the third sample, the SNR value of the iris probe image is almost six times that of the image generated by the circular probe, further highlighting the effectiveness of the probe to produce qualitatively and quantitatively better images when compared to a probe without the resonant iris structure.

The normalized magnitude and phase images for the fourth sample acquired using both probes are shown in Fig. 17. The localized corrosion under the paint layer is very sharply depicted in the magnitude as well as phase images generated by the iris probe, and is discernible from the background. While the corrosion under paint is visible in the images rendered by the circular aperture probe shown in Fig. 17(c) and (d), it is not as sharp and detailed as seen in the iris probe image. The outline of the localized corrosion is better illustrated in the iris probe image owing to its higher resolution and sensitivity. Furthermore, the SNR value of the iris probe image is almost twice that of the image rendered by the circular probe, as presented in Table 4. In conclusion, the qualitatively and quantitatively better images of the iris probe for both samples signifies the imaging capability of the probe in corrosion mapping.

To further demonstrate the effectiveness of the probe when compared to the probe introduced in [45], the images

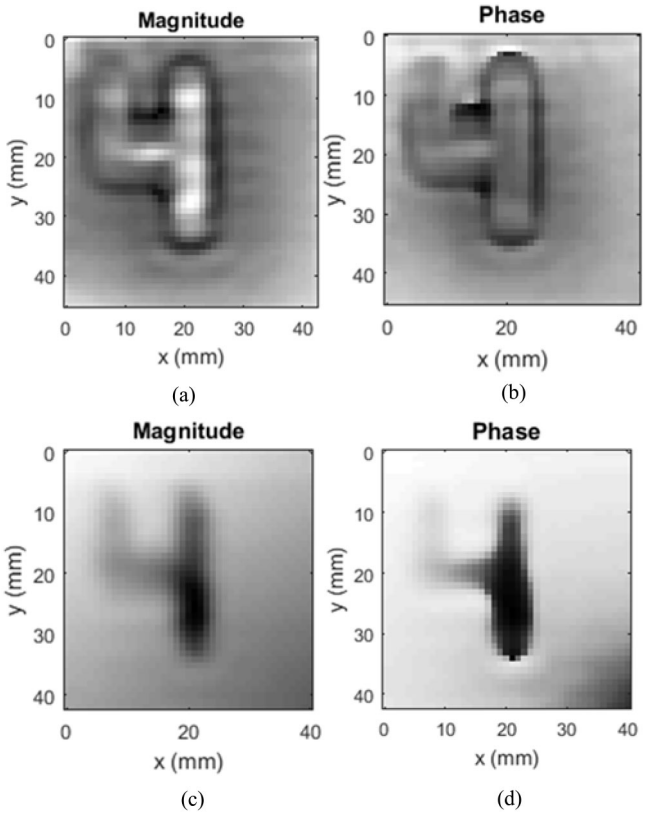

FIGURE 16. Normalized magnitude and phase images of corrosion Sample-3 obtained using (a, b) the proposed iris probe and (c, d) a circular aperture probe.

TABLE 4. SNR values of corrosion sample images.

Sample	Iris probe	Circular probe	Probe introduced in [45]
Sample-3	50.5	8.7	-
Sample-4	74.8	37.5	41.1

produced by the probe (in [45]) for sample-4 are also included in Fig. 17(e) and (f). The magnitude and phase image generated using this the probe does not faithfully render the corrosion under paint. Clearly, in the magnitude image, the corrosion is almost indistinguishable from the background. On the other hand, the probe proposed in this paper provided considerable improvement in terms of the sensitivity in this particular application. To compare the performance of the probes quantitatively, the SNR value of the probe introduced in [45] was computed. The obtained SNR value of 41.1 is still significantly less than the SNR of the proposed probe (74.8). Thus, the proposed probe qualitatively and quantitatively outperformed the probe used in [45]. It is remarked that the inadequacy of the previous probe to reliably detect corrosion under paint prompted the development of the high frequency iris probe proposed herein.

Besides the circular probe which was used herein for benchmarking, the proposed probe performs well in comparison to several other reported probes as listed in Table 5.

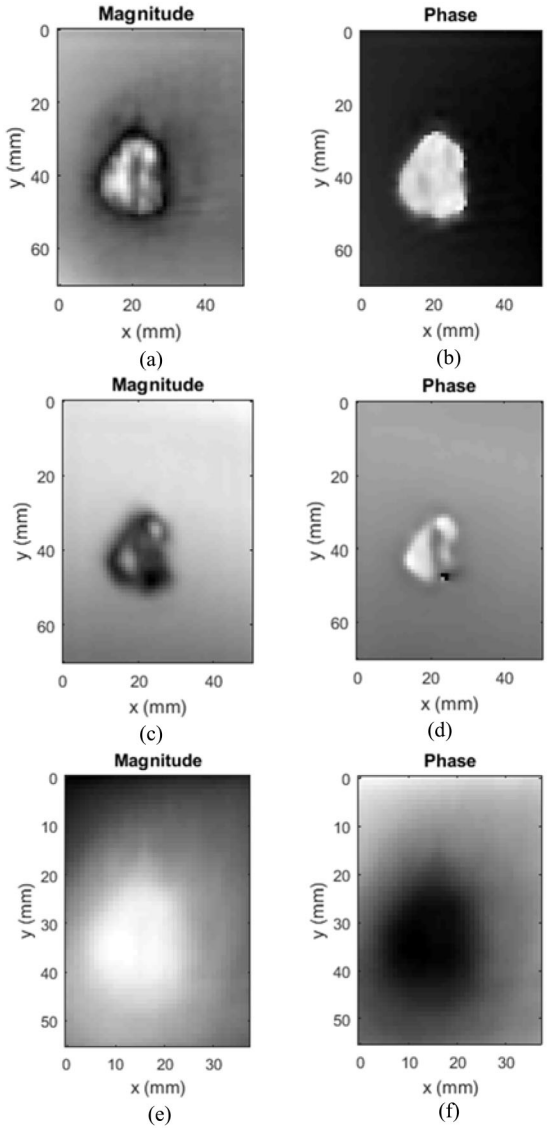

FIGURE 17. Normalized magnitude and phase images of the corrosion Sample-4 obtained using (a, b) the proposed iris probe, (c, d) a circular aperture probe and (e, f) the probe introduced in [45].

Evidently, the resolution obtained in this work is higher than most of the compared probes. Only the modified rectangular aperture probe with choke proposed in [58] achieved slightly better resolution. However, it is remarked here that the operating frequency of the rectangular aperture probe with choke was 80 GHz in the W-band with aperture broad dimension of 2.54 mm, which would inherently provide a resolution of less than 2 mm. Although a resolution of 2 mm was reported in [36] at a relatively lower frequency than the proposed probe, the results were obtained using an array of split ring resonators operating at small standoff distance of 0.6 mm. It is noted here that only a few previously developed probes were designed and optimized for crack detection while no imaging results were presented (except in [24]) to elucidate the sensitivity/practicability of the probe towards any other defect types like corrosion beneath a layer of paint.

TABLE 5. Resolution comparison against various probes.

Ref.	Resolution (mm)	SOD (mm)	Probe Type	Freq. (GHz)
[30]	4	1	Circular aperture probe	24
[24]	3	1	Planar resonator probe	0.78
[59]	2.5	1	Complementary spiral resonators	0.39
[57]	5	1	Coaxial resonator sensor	1.96
[58]	1.9	1	Rectangular aperture with choke	80
[34]	5	4	Helix probe	4
[17]	5	1	Planar resonator probe	0.426
[36]	2	0.6	Rectangular aperture with array of split ring resonators	14.67
This work	2	1	Circular aperture loaded with resonant iris	26

IV. CONCLUSION

A loaded circular aperture probe operating at 26 GHz has been introduced in this paper for high resolution imaging in the near-field area. The design of the iris structure was presented and the utility of the probe for crack detection and corrosion mapping was demonstrated. Extensive 3D electromagnetic simulations were conducted to analyze the probe performance and establish the spatial resolution of the probe. Subsequently, the resolution 'was confirmed through measurements on a similar sample. Attributes of the probe such as sensitivity and resolution were demonstrated experimentally and benchmarked against circular aperture probe without the resonant iris. It was shown that the loaded probe rendered better resolution and nearly six times more sensitive response for a narrow crack of width 0.25 mm. Furthermore, to highlight the effectiveness of the probe towards detection of corrosion under paint, simulations were performed for a uniform corrosion layer of varying thickness concealed under paint. The response was compared to a circular probe and it was shown that the iris probe was highly sensitive in terms of corrosion detection under paint for very small thicknesses. In addition to this, two practical corrosion under paint samples were imaged using the proposed probe and the high resolution images of the corrosion samples clearly showed the potential of the probe in industrial applications concerning inspection.

REFERENCES

[1] C.-Y. Yeh and R. Zoughi, "A novel microwave method for detection of long surface cracks in metals," *IEEE Trans. Instrum. Meas.*, vol. 43, no. 5, pp. 719–725, Oct. 1994.

[2] X. Yang *et al.*, "Array waveguide probe loaded with split-ring resonators for sizing the cracks in metal surface," *IEEE Microw. Wireless Compon. Lett.*, vol. 28, no. 2, pp. 171–173, Feb. 2018.

[3] M. S. Rahman, A. A. Mustapha, and M. A. Abou-Khousa, "Detection and sizing of surface cracks in metals using UHF probe," in *Proc. IEEE Int. Conf. Imag. Syst. Techn. (IST)*, 2021, pp. 1–5.

[4] A. M. Albishi, M. S. Boybay, and O. M. Ramahi, "Complementary split-ring resonator for crack detection in metallic surfaces," *IEEE Microw. Wireless Compon. Lett.*, vol. 22, no. 6, pp. 330–332, Jun. 2012.

[5] A. K. Rajni and A. Marwaha, "Detection of sub-millimeter crack on metal surface using complementary spiral resonator," *Int. J. Appl. Eng. Res.*, vol. 10, no. 9, pp. 24025–24036, 2015.

[6] C. Huber, H. Abiri, S. I. Ganchev, and R. Zoughi, "Modeling of surface hairline-crack detection in metals under coatings using an open-ended rectangular waveguide," *IEEE Trans. Microw. Theory Techn.*, vol. 45, no. 11, pp. 2049–2057, Nov. 1997.

[7] Q. Wang *et al.*, "High-sensitivity dielectric resonator-based waveguide sensor for crack detection on metallic surfaces," *IEEE Sensors J.*, vol. 19, no. 14, pp. 5470–5474, Jul. 2019.

[8] J. R. Gallion and R. Zoughi, "Millimeter-wave imaging of surface-breaking cracks in steel with severe surface corrosion," *IEEE Trans. Instrum. Meas.*, vol. 66, no. 10, pp. 2789–2791, Oct. 2017.

[9] M. A. Abou-Khousa and M. S. Ur Rahman, "Covered cracks detection using dual-polarization synthetic aperture radar imaging," *IEEE Trans. Instrum. Meas.*, vol. 70, pp. 1–4, Jun. 2021.

[10] M. T. Ghasr, S. Kharkovsky, R. Zoughi, and R. Austin, "Comparison of near-field millimeter-wave probes for detecting corrosion precursor pitting under paint," *IEEE Trans. Instrum. Meas.*, vol. 54, no. 4, pp. 1497–1504, Aug. 2005.

[11] M. T. Ghasr, B. Carroll, S. Kharkovsky, R. Austin, and R. Zoughi, "Millimeter-wave differential probe for nondestructive detection of corrosion precursor pitting," *IEEE Trans. Instrum. Meas.*, vol. 55, no. 5, pp. 1620–1627, Oct. 2006.

[12] M. S. Ur Rahman and M. A. Abou-Khousa, "Millimeter wave imaging of surface defects and corrosion under paint using V-band reflectometer," in *Proc. IEEE Int. Conf. Imag. Syst. Techn. (IST)*, 2019, pp. 1–5.

[13] N. N. Qaddoumi, W. M. Saleh, and M. Abou-Khousa, "Innovative near-field microwave nondestructive testing of corroded metallic structures utilizing open-ended rectangular waveguide probes," *IEEE Trans. Instrum. Meas.*, vol. 56, no. 5, pp. 1961–1966, Oct. 2007.

[14] M. S. Ur Rahman, A. Yassin, and M. A. Abou-Khousa, "Microwave imaging of thick composite structures using circular aperture probe," *Meas. Sci. Technol.*, vol. 29, no. 9, pp. 1–10, 2018.

[15] M. S. Ur Rahman, A. A. Mustapha, and M. A. Abou-Khousa, "Millimeter-wave SAR imaging of composites using rectangular aperture probe," in *Proc. IEEE Int. Conf. Imag. Syst. Techn. (IST)*, 2021, pp. 1–6.

[16] A. Yassin, M. S. Ur Rahman, and M. A. Abou-Khousa, "Imaging of near-surface defects using microwaves and ultrasonic phased array techniques," *J. Nondestruct. Eval.*, vol. 37, no. 71, pp. 1–8, 2018.

[17] M. A. Abou-Khousa, K. T. M. Shafi, and X. Xingyu, "High-resolution UHF near-field imaging probe," *IEEE Trans. Instrum. Meas.*, vol. 67, no. 10, pp. 2353–2362, Oct. 2018.

[18] J. Baker-Jarvis, M. D. Janezic, P. D. Domich, and R. G. Geyer, "Analysis of an open-ended coaxial probe with lift-off for nondestructive testing," *IEEE Trans. Instrum. Meas.*, vol. 43, no. 5, pp. 711–718, Oct. 1994.

[19] D. M. Hagl, D. Popovic, S. C. Hagness, J. H. Booske, and M. Okoniewski, "Sensing volume of open-ended coaxial probes for dielectric characterization of breast tissue at microwave frequencies," *IEEE Trans. Microw. Theory Techn.*, vol. 51, no. 4, pp. 1194–1206, Apr. 2003.

[20] M. S. Boybay and O. M. Ramahi, "Open-ended coaxial line probes with negative permittivity materials," *IEEE Trans. Antennas Propag.*, vol. 59, no. 5, pp. 1765–1769, May 2011.

[21] G. Govind, N. K. Tiwari, K. K. Agarwal, and M. J. Akhtar, "Microwave subsurface imaging of composite structures using complementary split ring resonators," *IEEE Sensors J.*, vol. 18, no. 18, pp. 7442–7449, Sep. 2018.

[22] N. K. Tiwari, S. P. Singh, and M. J. Akhtar, "Near field planar microwave probe sensor for nondestructive condition assessment of wood products," *J. Appl. Phys.*, vol. 123, pp. 1–9, May 2018.

[23] A. Ali, M. El Badawe, and O. M. Ramahi, "Microwave imaging of subsurface flaws in coated metallic structures using complementary split-ring resonators," *IEEE Sensors J.*, vol. 16, no. 18, pp. 6890–6898, Sep. 2016.

[24] A. Haryono, K. Al-Jaberi, M. S. Ur Rahman, and M. A. Abou-Khousa, "High resolution and polarization independent microwave near-field imaging using planar resonator probes," *IEEE Access*, vol. 8, pp. 191421–191432, 2020.

[25] M. A. Abou-Khousa and A. Haryono, "Array of planar resonator probes for rapid near-field microwave imaging," *IEEE Trans. Instrum. Meas.*, vol. 69, no. 6, pp. 3838–3846, Jun. 2020.

[26] G. Wang, J. Fang, and X. Dong, "Resolution of near-field microwave target detection and imaging by using flat LHM lens," *IEEE Trans. Antennas Propag.*, vol. 55, no. 12, pp. 3534–3541, Dec. 2007.

[27] J. T. Shen and P. M. Platzman, "Near field imaging with negative dielectric constant lenses," *Appl. Phys. Lett.*, vol. 80, no. 18, pp. 3286–3288, 2002.

[28] M. F. Imani and A. Grbic, "Planar near-field plates," *IEEE Trans. Antennas Propag.*, vol. 61, no. 11, pp. 5425–5434, Nov. 2013.

[29] A. Grbic and R. Merlin, "Near-field focusing plates and their design," *IEEE Trans. Antennas Propag.*, vol. 56, no. 10, pp. 3159–3165, Oct. 2008.

[30] M. R. Ramzi, M. A. Abou-Khousa, and I. Prayudi, "Near-field microwave imaging using open-ended circular waveguide probes," *IEEE Sensors J.*, vol. 17, no. 8, pp. 2359–2366, Apr. 2017.

[31] K. Chan, K. Rambabu, and P. Boulanger, "Open-ended waveguide dielectric probe using time-domain measurements," *Microw. Opt. Technol. Lett.*, vol. 60, no. 5, pp. 1108–1112, 2018.

[32] A. Taeb, S. Gigoyan, and S. Safavi-Naeini, "Millimetre-wave waveguide reflectometers for early detection of skin cancer," *IET Microw. Antennas Propag.*, vol. 7, no. 14, pp. 1182–1186, 2013.

[33] O. Malyuskin and V. Fusco, "Near field enhancement and subwavelength imaging using resonantly loaded apertures," *IEEE Trans. Antennas Propag.*, vol. 62, no. 6, pp. 3130–3140, Jun. 2014.

[34] O. Malyuskin and V. F. Fusco, "High-resolution microwave near-field surface imaging using resonance probes," *IEEE Trans. Instrum. Meas.*, vol. 65, no. 1, pp. 189–200, Jan. 2016.

[35] V. Fusco and O. Malyuskin, "Resonantly loaded apertures for high-resolution near-field surface imaging," *IET Sci. Meas. Technol.*, vol. 9, no. 7, pp. 783–791, 2015.

[36] B. Hu, Z. Ren, M. S. Boybay, and O. M. Ramahi, "Waveguide probe loaded with split-ring resonators for crack detection in metallic surfaces," *IEEE Trans. Microw. Theory Techn.*, vol. 62, no. 4, pp. 871–878, Apr. 2014.

[37] M. A. Abou-Khousa, M. S. U. Rahman, and X. Xingyu, "Dual-polarized microwave imaging probe," *IEEE Sensors J.*, vol. 19, no. 5, pp. 1767–1776, Mar. 2019.

[38] N. N. Qaddoumi, M. A. Abou-Khousa, and W. M. Saleh, "Near-field microwave imaging utilizing tapered rectangular waveguides," *IEEE Trans. Instrum. Meas.*, vol. 55, no. 5, pp. 1752–1756, Oct. 2006.

[39] M. A. Abou-Khousa, S. Kharkovsky, and R. Zoughi, "Novel near-field millimeter-wave differential probe using a loaded modulated aperture," *IEEE Trans. Instrum. Meas.*, vol. 58, no. 5, pp. 1273–1282, May 2009.

[40] S. Dieter and W. Menzel, "High-resolution probes for near-field measurements of reflectarray antennas," *IEEE Antennas Wireless Propag. Lett.*, vol. 8, pp. 157–160, 2009.

[41] S. Kharkovsky, A. McClanahan, R. Zoughi, and D. D. Palmer, "Microwave dielectric-loaded rectangular waveguide resonator for depth evaluation of shallow flaws in metals," *IEEE Trans. Instrum. Meas.*, vol. 60, no. 12, pp. 3923–3930, Dec. 2011.

[42] K. Haddadi and T. Lasri, "60-GHz near-field six-port microscope using a scanning slit probe for subsurface sensing," *IEEE Sensors J.*, vol. 12, no. 8, pp. 2575–2576, Aug. 2012.

[43] H.-W. Son and Y.-K. Cho, "Two types of near-field microwave imaging probes," in *Proc. 31st URSI Gen. Assem. Sci. Symp. (URSI GASS)*, vol. 1, 2014, pp. 1–4.

[44] M. A. Abou-Khousa, S. Kharkovsky, and R. Zoughi, "On the mutual coupling between circular resonant slots," in *Proc. 3rd Int. Conf. Electromagn. Near-Field Characterization Imag. (ICONIC)*, St. Louis, MO, USA, 2007, pp. 1–6.

[45] M. S. Ur Rahman, K. Al-Wahedi, and M. A. Abou-Khousa, "Microwave resonant loaded probe for non-destructive evaluation of multilayer composites," *J. Nondestruct. Eval.*, vol. 41, pp. 1–9, Nov. 2021.

[46] "CST-computer simulation technology." 2022. [Online]. Available: http://www.cst.com

[47] T. Y. Otoshi, R. Cirillo, Jr., and J. Sosnowski, "Measurements of complex dielectric constants of paints and primers for DSN antennas: Part I," Telecommun. Mission Oper., TMO Progress Rep. 42–138, 1999.

[48] M. A. Abou-Khousa, A. Al-Durra, and K. Al-Wahedi, "Microwave sensing system for real-time monitoring of solid contaminants in gas flows," *IEEE Sensors J.*, vol. 15, no. 9, pp. 5296–5302, Sep. 2015.
[49] J. Kerouedan, P. Quéffélec, P. Talbot, C. Quendo, S. De Blasi, and A. Le Brun, "Detection of micro-cracks on metal surfaces using near-field microwave dual-behavior resonator filters," *Meas. Sci. Technol.*, vol. 19, no. 10, 2008, Art. no. 105701.
[50] S.-H. Yang, K.-B. Kim, and J.-S. Kang, "Detection of surface crack in film-coated metals using an open-ended coaxial line sensor and dual microwave frequencies," *NDT E Int.*, vol. 54, pp. 91–95, Mar. 2013.
[51] A. M. Yadegari, R. Moini, S. H. H. Sadeghi, and F. Mazlumi, "Output signal prediction of an open-ended rectangular waveguide probe when scanning cracks at a non-zero lift-off," *NDT E Int.*, vol. 43, pp. 1–7, Jan. 2010.
[52] A. McClanahan, S. Kharkovsky, A. R. Maxon, R. Zoughi, and D. D. Palmer, "Depth evaluation of shallow surface cracks in metals using rectangular waveguides at millimeter-wave frequencies," *IEEE Trans. Instrum. Meas.*, vol. 59, no. 6, pp. 1693–1704, Jun. 2010.
[53] I. Ahanian, S. H. H. Sadeghi, and R. Moini, "An array waveguide probe for detection, location and sizing of surface cracks in metals," *NDT E Int.*, vol. 70, pp. 38–40, Mar. 2015.
[54] T. Yun and S. Lim, "High-Q and miniaturized complementary split ring resonator-loaded substrate integrated waveguide microwave sensor for crack detection in metallic materials," *Sens. Actuat. A, Phys.*, vol. 214, pp. 25–30, Aug. 2014.
[55] S. Kharkovsky, M. T. Ghasr, and R. Zoughi, "Near-field millimeter-wave imaging of exposed and covered fatigue cracks," *IEEE Trans. Instrum. Meas.*, vol. 58, no. 7, pp. 2367–2370, Jul. 2009.
[56] R. Zoughi and S. Kharkovsky, "Microwave and millimetre wave sensors for crack detection," *Fatigure Fract. Eng. Mater. Struct.*, vol. 31, pp. 695–713, Oct. 2008.
[57] H. Zhou, Q. Zhang, and R. D. Murch, "Frequency-diverse near-field sensing using multiple coupled-resonator probes," *IEEE Trans. Microw. Theory Techn.*, vol. 68, no. 10, pp. 4455–4465, Oct. 2020.
[58] A. Baskakova and K. Hoffmann, "W-Band imaging sensor using a rectangular waveguide structure with choke," *IEEE Microw. Wireless Compon. Lett.*, vol. 32, no. 3, pp. 230–233, Mar. 2022.
[59] Z. Xie, Y. Li, L. Sun, W. Wu, R. Cao, and X. Tao, "A simple high-resolution near-field probe for microwave non-destructive test and imaging," *Sensors*, vol. 20, no. 9, p. 2670, 2020.

MOHAMMED SAIF UR RAHMAN received the B.S. degree in instrumentation engineering from Osmania University, Hyderabad, India, in 2011, and the M.S. degree in control and instrumentation engineering from King Fahd University, Dhahran, Saudi Arabia, in 2015.

He is currently working as a Research Associate with the Smart Sensing Systems Group, Khalifa University of Science and Technology, Abu Dhabi, UAE. His research interests include instrumentation, sensing systems, non-destructive testing, and microwave imaging.

OMAR S. HASSAN graduated with distinguished honors and a major focus in the communication field from the Electrical Engineering Department, Ajman University, Fujairah, UAE, in 2015, and the M.S. degree in electrical and computer engineering from Khalifa University, Abu Dhabi, UAE, in 2022, with research focus in antenna design, space communication, RF measurement, and imaging.

MOHAMED A. ABOU-KHOUSA (Senior Member, IEEE) received the B.S. degree (*magna cum laude*) from the American University of Sharjah, Sharjah, UAE, in 2003, the M.S. degree from Concordia University, Montreal, QC, Canada, in 2004, and the Ph.D. degree from the Missouri University of Science and Technology (Missouri S&T), Rolla, MO, USA, in 2009, all in electrical engineering. From 2005 to 2009, he was a Graduate Research Assistant with the Applied Microwave Nondestructive Testing Laboratory, Missouri S&T. He was a Research Scientist/Engineer with Robarts Research Institute, London, ON, Canada, from 2009 to 2013. He is currently an Associate Professor with the Electrical Engineering and Computer Science Department, Khalifa University of Science and Technology, Abu Dhabi, UAE. His areas of expertise include RF, microwave, and millimeter-wave instrumentation, material characterization, nondestructive testing, and subsurface imaging. Over the course of his career, he executed various research and development projects within broad range of sectors, including oil and gas, biomedical, space, and aerospace. He has coauthored many technical publications in his areas of expertise, and has to his credit several patents. He is the recipient of multiple national and international awards, including the IEEE Instrumentation and Measurement Society 2017 Outstanding Young Engineer Award. As a coauthor, he was a recipient of the H. A. Wheeler Applications Prize Paper Award from the IEEE Antennas and Propagation Society. He currently serves as an Associate Editor-in-Chief for the IEEE TRANSACTIONS ON INSTRUMENTATION AND MEASUREMENT.